Design of a biased potent small molecule inhibitor of the bromodomain and PHD finger-containing (BRPF) proteins suitable for cellular and *in vivo* studies

Niall Igoe,[a] Elliott D. Bayle,[a] Oleg Fedorov,[b] Cynthia Tallant,[b] Pavel Saitsky,[b] Catherine Rogers,[b] Dafydd R. Owen,[c] Gauri Deb,[d] Tim C. P. Somervaille, [d] David M. Andrews,[e] Neil Jones,[f] Anne Cheasty,[f] Hamish Ryder,[f] Paul E. Brennan,[b] Susanne Müller,[b,g] Stefan Knapp,[b,g,h] and Paul V. Fish [a,]*

[a] UCL School of Pharmacy, 29/39 Brunswick Square, London, WC1N 1AX, UK

[b] Nuffield Department of Clinical Medicine, Structural Genomics Consortium, University of Oxford, Old Road Campus Research Building, Roosevelt Drive, Oxford, OX3 7DQ, UK

[c] Pfizer Worldwide Medicinal Chemistry, 610 Main Street, Cambridge, MA 02139, USA

[d] Leukemia Biology Laboratory, Cancer Research UK Manchester Institute, Manchester M20 4BX, UK

[e] AstraZeneca Discovery Sciences, Darwin Building, Cambridge Science Park, Cambridge CB4 0FZ, UK

[f] CRT Discovery Laboratories, Jonas Webb Building, Babraham Research Campus, Cambridge CB22 3AT, UK

[g] Buchmann Institute for Molecular Life Sciences, Max-von-Laue-Strasse 15, D-60438 Frankfurt am Main, DE

[h] Institute for Pharmaceutical Chemistry, Johann Wolfgang Goethe-University, Max-von-Laue-Strasse 9, D-60438 Frankfurt am Main, DE

ABSTRACT: The BRPF (bromodomain and PHD finger-containing) family are scaffolding proteins important for the recruitment of histone acetyltransferases of the MYST family to chromatin. Evaluation of the BRPF family as a potential drug target is at an early stage although there is an emerging understanding of a role in acute myeloid leukemia (AML). We report the optimization of

fragment hit **5b** to **13-d** as a biased, potent inhibitor of the BRD of the BRPFs with excellent selectivity over non-class IV BRD proteins. Evaluation of **13-d** in a panel of cancer cell lines showed a selective inhibition of proliferation of a subset of AML lines. Pharmacokinetic studies established that **13-d** had properties compatible with oral dosing in mouse models of disease (F_{po} 49 %). We propose that **NI-42** (**13-d**) is a new chemical probe for the BRPFs suitable for cellular and *in vivo* studies to explore the fundamental biology of these proteins.

KEYWORDS: BRPF1, BRPF2, BRD1, BRPF3, BRD7, BRD9, ATAD2, BET, bromodomain, fragment hit, chemical probe, NI-42, acute myeloid leukemia.

INTRODUCTION

Bromodomains (BRDs) are protein interaction modules that bind to acetylated lysine containing sequence motifs on chromatin and non-chromatin proteins, and act as epigenetic reader domains.[1] Despite large sequence variations, bromodomains share a conserved fold with a central deep, largely hydrophobic acetyl-lysine (Ac-Lys) binding pocket, which for many family members is considered highly druggable.[2] Accordingly, since the publication of the first bromodomain inhibitors of the Bromodomain and extra-terminal (BET) family in 2010,[3,4] inhibitors for the major branches of the bromodomain family tree have been generated.[5] Importantly, for many of the bromodomains more than one inhibitor, from alternative scaffolds are available, providing confidence in the observed biological results.[6,7] In addition, structurally related compounds that don't bind to the respective bromodomain often complement the inhibitor package lending credibility to the observed findings.[3,8,9]

In human, 61 bromodomains are present in 46 proteins and some exist as alternatively spliced forms.[10] The bromodomain and PHD finger-containing (BRPF) protein family of bromodomains contains four members. BRPF1A and BRPF1B are generated by alternative splicing resulting in a longer BRPF1A isoform, which has a 6 residue insert in the BRD, and the shorter BRPF1B isoform.[10] The related BRPF2 (also termed BRD1) and BRPF3 proteins share the general domain structure with BRPF1A and 1B comprising a double PHD and zinc finger arrangement, a bromodomain, and a C-terminal chromo/Tudor-related PWWP domain. The PWWP domain of BRPF1 binds to trimethylated Lys36 in histone H3 (H3K36me3) and is important for targeting BRPF1 to chromatin,[11] while the BRD of BRPF1 recognizes multiple Ac-Lys modifications on the N-terminal histone tail, in particular H2AK5ac, H4K12ac, and H3K14ac.[12] This modular arrangement points to a role of the BRPF family members as scaffolding proteins. Indeed, BRPFs are found in a tetrameric complex with ING5 and Eaf6/EPC-related scaffold subunit, as well as one of the MYST family members of the H3K9 and H3K14 histone acetyl transferases (HATs): MOZ or MORF; or alternatively HBO1 in case of BRPF2/3.[13] Interestingly, BRPF1 can also associate with HBO1 resulting in a switch from the commonly preferred substrate H4 to H3.[14]

Chromosomal translocations that involve the MOZ gene are associated with acute myeloid leukemia (AML) and overexpression of HOXA9 and HOXA10 was observed in AML patients with MOZ fusions.[15] BRPF1 is a core component of MOZ/MORF HAT complexes with a key role in their

assembly and activation,[16] and facilitates interaction with chromatin. BRPF1 is essential for the proper formation of fetal hematopoietic stem cells as well as expression of stem cell genes such as *Hoxa9.*[17] In AML, MOZ is recurrently targeted by chromosomal translocations and the resulting fusion oncoproteins (e.g. MOZ-TIF2) form a stable complex with BRPF1 which interacts with, and deregulates, HOX gene loci.[18] Conversely, depletion of BRPF1 decreased the MOZ localisation on HOX genes abrogating transformation, and mutant MOZ-TIF2 engineered to lack HAT activity was incapable of deregulation of HOX genes or initiating leukemia.[18] These data indicate that the MOZ-TIF2/BRPF1 complex upregulates HOX gene expression possibly mediated by MOZ-dependent histone acetylation, leading to development of leukemia.[18]

Further evidence supporting BRPF1 as a credible target for AML includes: (1) its expression is highest in acute leukemia cell lines versus all other cell line types;[19] (2) the normal role of BRPF1 is to sustain HOX gene expression in development[18] and misregulated HOX gene expression is critical to the pathogenesis of at least 70% of AML, in particular the MLL mutated subtypes and AMLs with mutations in NPM1;[20] (3) BRPF1 has significant homology with AF10 and AF17, two recurrent fusion partners of MLL in human AML;[21] and (4) the complex formed by BRPF1, ING5 and MOZ binds to, and acetylates, histone H3 to act as a co-activator of RUNX1, which is another critical transcriptional regulator in AML.[22]

Hence, this emerging body of evidence supports the potential role of BRPF1 in leukemia and prompted us to explore AML as a pathfinder cancer disease. Targeting the MYST complex by inhibition of BRPF1B provides a potential therapeutic opportunity in AML, although deletion of the BRPF1 bromodomain does not prevent the acetylation of histone H3 by the HBO1/BRPF1 complex.[14]

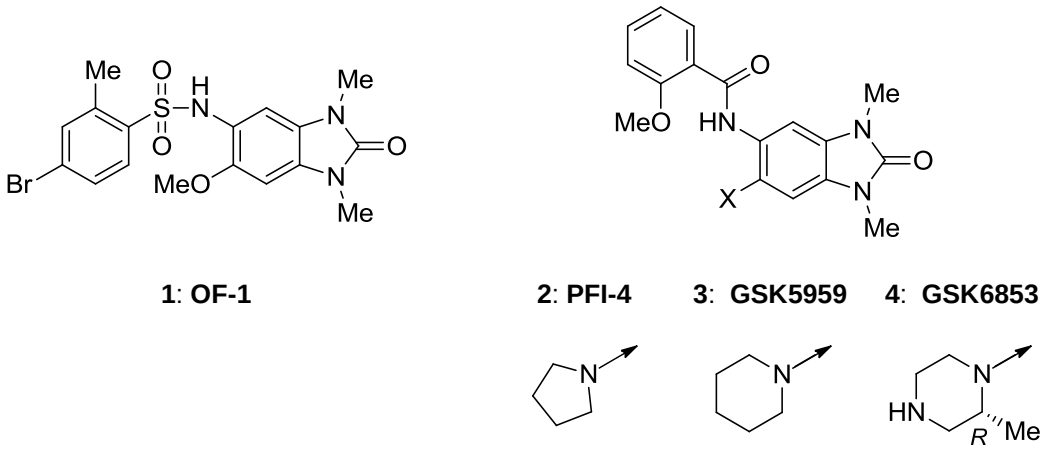

Figure 1: 1,3-Dimethyl benzimidazolones as inhibitors of the bromodomain of the BRPFs.

Contemporaneous studies identified the 1,3-dimethyl benzimidazolone template as binding to the BRD of BRPF1[6,7] and this core has been independently optimised to give three chemical probes as either the pan-BRPF BRD inhibitor OF-1 (**1**),[23] or as the selective BRPF1 BRD inhibitors PFI-4 (**2**)[24] and GSK5959 (**3**)[25] which share a very similar chemical structure (Figure 1). Piperidine **3** has been further optimised to the α-methyl piperazine analogue GSK6853 (**4**) which has significantly improved solubility, and properties suitable for cellular and *in vivo* dosing, albeit by *ip* administration.[26] The 1,3-dimethyl benzimidazolone template has also been used to identify selective TRIM24-BRPF1B dual inhibitors.[27]

The use of selective small molecule inhibitors as chemical probes to investigate the relationship between the target and disease is significantly enhanced when two structurally orthogonal chemical probes are employed. Two different chemotypes which share the same primary pharmacology are likely to offer the advantage of a different secondary pharmacology fingerprint profile and so help identify any off-target effects in cellular assays.

Our aims were to discover new small molecule inhibitors of the BRD of the BRPFs to explore the fundamental biology of these proteins and then build target validation to underpin new drug discovery programs. Ideally these small molecule inhibitors would be suitable for oral dosing in *in vivo* model of disease and have drug-like properties. Here we report **13-d** as a new, structurally orthogonal chemical probe for the BRPFs suitable for cellular and *in vivo* studies.

RESULTS AND DISCUSSION

Origin of Quinolin-2-one Hit Series. The starting point was fragment hit *N*-methylquinolin-2(1*H*)-one (**5b**) which was originally identified as binding to PCAF (Figure 2).[28] In fact, quinolin-2-ones **5a** and **5b** have proven to be efficient and versatile fragment hits for a number of BRDs and further optimization has identified potent inhibitors and chemical probes for the BETs,[29] BRD7/9,[30] and ATAD2.[31] However, our analysis of quinolin-2-one **5b** showed it to be a more potent inhibitor of BRPF1 (IC_{50} 4800 nM) when compared to other BRDs which have been investigated (Table 1).

Figure 2: Evolution of *N*-methylquinolin-2(1*H*)-ones as BRPF inhibitors

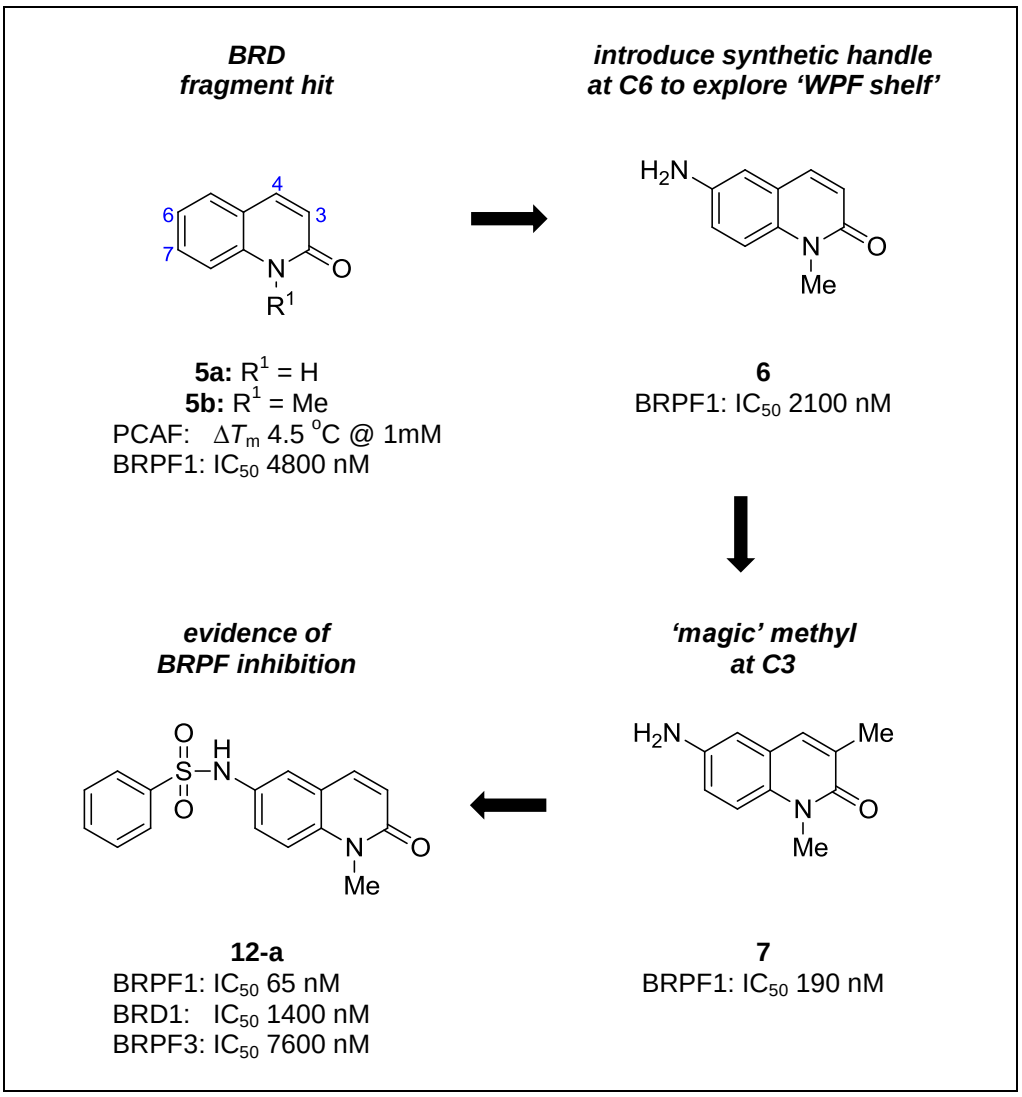

Table 1. Inhibition of BRD activity by fragment hit 5b.[a]

BRD	IC_{50} (nM)
BRPF1	4800
BRD9	14,000
PCAF	70,000
BRD4(BD1)	73,000
ATAD2	>100,000

[a] BROMO*scan* assay. BRD IC_{50} values are geometric means of two experiments. Differences of <2-fold should not be considered significant.

Hence **5b** was selected as our starting point for several reasons: (1) excellent 'hit-like' properties (mw 159; cLogP 1.3; LE = 0.62; LLE = 4.0) with no obvious reactive groups; (2) evidence that selectivity between BRDs could be achieved and, in particular, over BET family member BRD4; (3) chemically enabled with sufficient synthetic chemistry precedent to selectively functionalize each position of the template to explore and establish SAR to guide optimization; and (4) a co-crystal structure of BRPF1B was solved to support compound design.

We determined the x-ray co-crystal structure of fragment **5b** bound to BRPF1B. As predicted, the quinolin-2-one scaffold serves as the acetyl-lysine mimetic with the carbonyl forming a hydrogen bond to the conserved Asn708 at 2.9 Å and forming a water mediated hydrogen bond with Tyr665 (Figure 3). The aromatic core is stabilized with the hydrophobic residues at the ZA channel (Val657 and P658) and two residues at the lipophilic shelf adjacent to the ZA channel (Ile652 and Phe653). The quinolin-2-one fragment was not large enough to induce conformational changes to the binding site and to the Phe714 gatekeeper residue when compared with the ligand-free structure of BRPF1B.

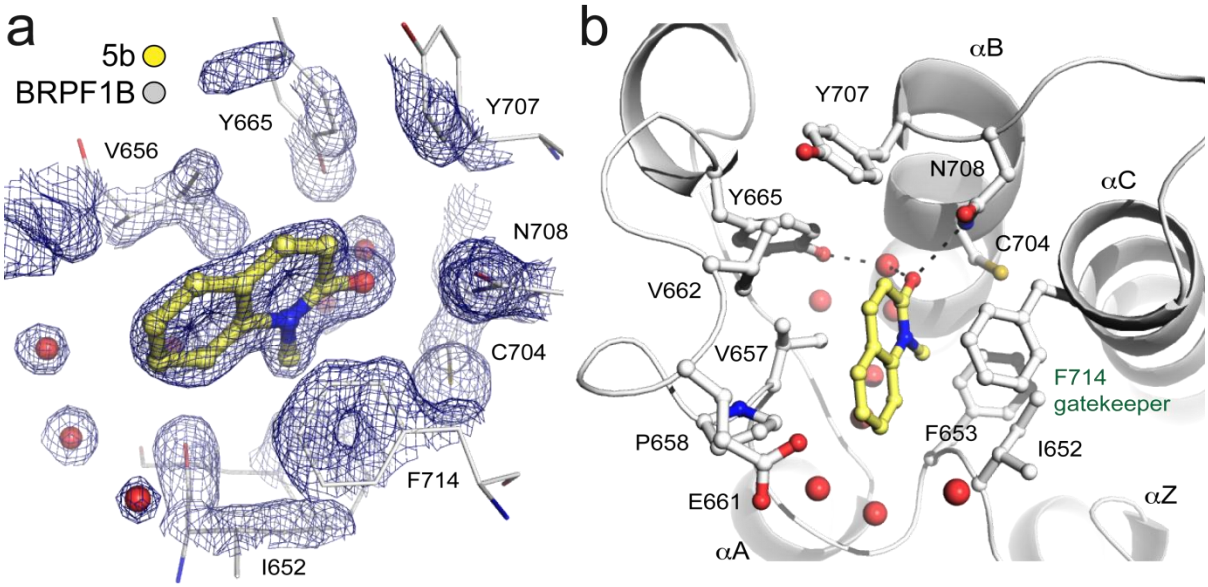

Figure 3. *N*-Methylquinolin-2(1*H*)-one (**5b** in yellow) co-crystallized with BRPF1B (grey) and solved at 1.5 Å (pdb 5T4U). A) 2Fo − Fc electron density map contoured at 1.2σ showing the **5b** inhibitor bound to BRPF1B. The figure shows the map for the fully refined structure. B) Binding site details of the **5b** ligand interaction.

Based on the affinity values (IC_{50}) obtained for **5b** among these bromodomains (Table 1), we superposed structures and aligned sequences (Figure S4) and observe that the binding specificity of **5b** is very sensitive to the nature of the gatekeeper residue, in which a rather bulky and hydrophobic residue is favourable. Also, a lipophilic residue at the ZA-loop (Pro658 for BRPF1B) is preferred to stabilize and sandwich the fragment at the binding site. The proline side chain is at 3.4 Å distance to the aromatic core of the quinolin-2-one, whereas other side chain residues in this position are pointing away to the binding site (Glu1014 for ATAD2; Thr50 for BRD9), or disordered side chains (Lys753 for PCAF).

Introduction of a 6-NH_2 into the quinolin-2-one template gave **6** which retained affinity whilst providing a functional group suitable for further elaboration to explore SAR. This 6-NH_2 group is positioned adjacent to the 'WPF shelf' region of the protein which is important for establishing selectivity between BRDs; the corresponding sequence in BRPF1 is Asn-Ile-Phe with Phe714 as the 'gate-keeper' residue. One of the most significant modifications was the introduction of a 3-Me group to give **7** as a potent fragment-like lead (BRPF1 IC_{50} 190 nM; mw 188; cLogP 0.95; LE = 0.67; LLE = 5.8). This methyl group enhanced affinity by 10-fold which is near to the maximum feasible from a buried Me group in an hydrophobic environment as assessed by binding energy calculations.[32] Using our co-

crystal structure of BRPF1B with **5b** as a model, the 3-Me of **7** was rationalised as projecting towards Y707 with the N1-Me fitting into the Me-pocket as employed by the Me groups of the Ac-Lys residues of the histone substrates (Figure S5).[33] Alternatively, the binding of **7** could also be accommodated by flipping the template about the C(2)=O axis and swapping the binding orientation of the 3-Me and N1-Me groups; both orientations would likely stabilize binding for **7** and improve affinity for BRPF1B when compared to **5b**.

Capping the 6-NH_2 group of **6** as a phenyl sulfonamide gave **12-a**. This modification introduced a bend into the molecule which gave the sulfonamide group the opportunity to turn out of the Ac-Lys binding pocket and wrap around the 'gate-keeper' Phe714. This binding mode would be quite different to the linear 5-carboxamides as used in **2** – **4** which project out past Phe714 towards the sidechain of Glu661. Preliminary results with the phenyl sulfonamide **12-a** were encouraging showing reasonable binding affinity for all three BRPFs with a preferred affinity for BRPF1 (IC_{50} 65 nM) whilst retaining good physicochemical properties (mw 314; cLogP 2.0; LE 0.46; LLE 5.2). Hence, we selected **12-a** as the lead for our SAR studies with the aim of improving binding affinity for the BRPFs whilst reducing affinity for other BRDs, especially BRD4.

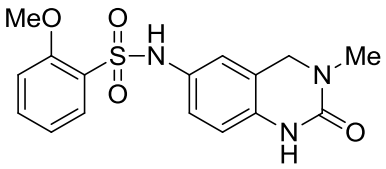

23: PFI-1

All non-BET BRD inhibitors need to demonstrate excellent selectivity over BRD4 because of the dominant phenotype of this protein in cellular models of disease due to the central role played in many biological pathways. The selection of quinolin-2-one sulfonamide **12-a** as our lead meant it was necessary for us to monitor selectivity over BRD4 as **12-a** shares some structural similarity with PFI-1 (**23**) a chemical probe for the BETs[34] which is a potent inhibitor of BRD4(BD1 and BD2) (IC_{50} 44 nM) and yet has weak BRPF1 affinity (IC_{50} 1800 nM).[29,35] We aimed to identify a prototype compound with a 1000-fold selectivity window for BRPF1 over BRD4 *and* a BRD4 affinity of IC_{50} > 5 μM to be used in cellular phenotypical assays at reasonable concentrations, and then adjust selectivity if required.

These criteria are far more stringent than the usual minimum selectivity requirements for chemical probes (30-fold)[8,36] but necessary to deliver a compound that would be 'fit-for-purpose' without an undercurrent of BRD4 activity to potentially confound biological results.

Chemistry. The general method for the synthesis of the quinolin-2(1*H*)-one sulfonamides **12**-**16** is outlined in Scheme 1. The 6-amino quinolin-2(1*H*)-ones **6**-**10** were reacted with the appropriate sulfonyl chlorides **11** in the presence of base to give the corresponding sulfonamides **12-16**. The amines **6**-**10** were prepared by published methods or the application of known procedures. The sulfonyl chlorides **11** were purchased from commercial sources or prepared by standard methods.

Scheme 1: General synthesis of sulfonamides **12**-**16**

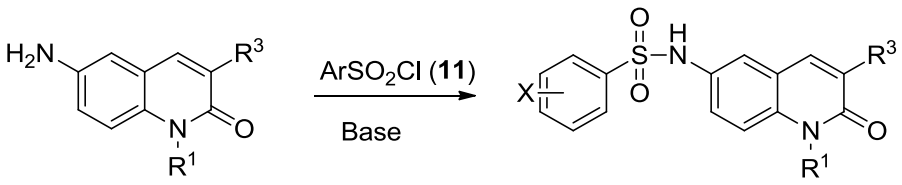

6:	R^1 = Me; R^3 = H	**12:**	R^1 = Me; R^3 = H
7:	R^1 = R^3 = Me	**13:**	R^1 = R^3 = Me
8:	R^1 = Me; R^3 = Et	**14:**	R^1 = Me; R^3 = Et
9:	R^1 = Et; R^3 = Me	**15:**	R^1 = Et; R^3 = Me
10:	R^1 = R^3 = Et	**16:**	R^1 = R^3 = Et

As the project developed, the need for larger amounts of material to support SAR studies prompted the development of an improved synthesis of 6-amino-1,3-dimethylquinolin-2(1*H*)-one (**7**)[37,38] (Scheme 2). This 5-step sequence was performed on multi-gram scale and represents a high-yielding, chromatography-free and operationally simple synthesis of **7**. 3-Methylquinoline (**17**) was converted to the corresponding 3-methylquinolin-2(1*H*)-one (**18**) by the two-step process of oxidation with *m*CPBA to the intermediate *N*-oxide followed by rearrangement and hydrolysis of the activated benzoyl ester with aq. NaOH. Selective *N*-methylation of **18** was achieved with NaH and MeI in DMF to give **19**, and nitration with KNO_3 in *conc.* H_2SO_4 gave **20** in high yield. Finally, reduction of the 6-NO_2 group was most conveniently achieved by catalytic hydrogenation to give amine **7**.

Scheme 2: Synthesis of 6-amino-1,3-dimethylquinolin-2(1*H*)-one (**7**) and **13-d**.

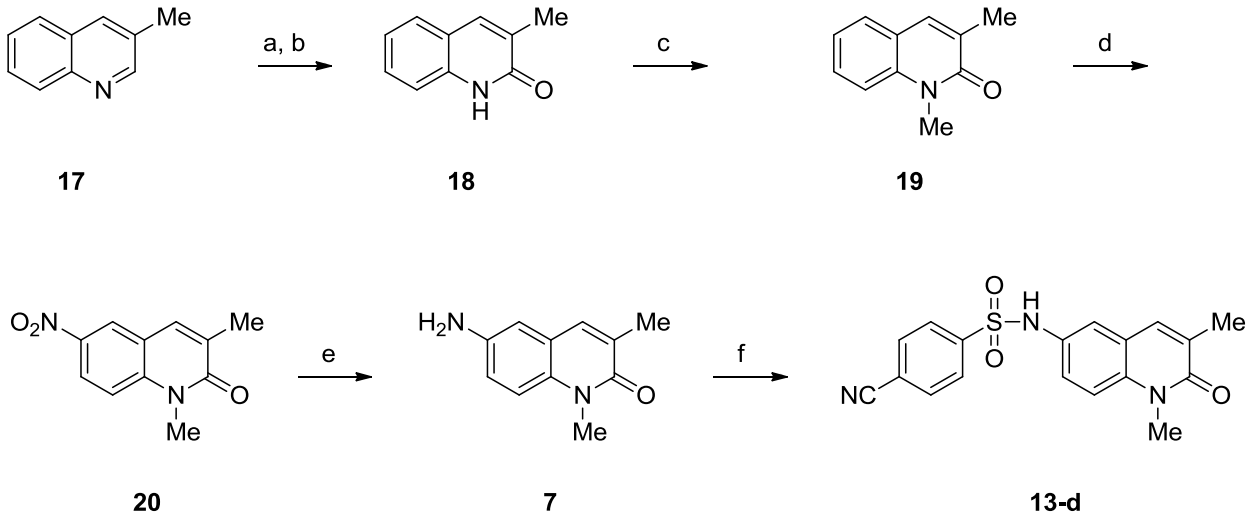

Reagents and Conditions: (a) *m*CPBA (1.1 eq), CH_2Cl_2, 0 $^oC \rightarrow$ rt, o/n; (b) C_6H_5COCl (1.2 eq), aq. NaOH (1.0 M), CH_2Cl_2, 0 $^oC \rightarrow$ rt, o/n, 59 % over two steps; (c) NaH (1.1 eq), MeI (1.3 eq), DMF, 0 $^oC \rightarrow$ rt, 5 h, 95 %; (d) *conc.* H_2SO_4, KNO_3 (1.05 eq), 0-5 $^oC \rightarrow$ rt, 4 h, 87 %; (e) H_2 (1 atmos), Pd/C (5 wt%, 0.05 eq), EtOH, rt, 7 h, 95 %; (f) 4-cyanobenzenesulfonyl chloride (1.0 eq), pyridine (2.0 eq), DMF, rt, o/n, 37-61 %.

The general method for the small-scale synthesis of sulfonamide test compounds **12**-**16** (typically 20-100 mg) was to react the amine with an excess of sulfonyl chloride (1.5 eq.) with pyridine (2.0 eq.) in CH_2Cl_2 or DMF at room temperature overnight, followed by evaporation of solvents and direct purification of the crude reaction mixture by chromatography. For larger amounts of material, the amine was coupled with the sulfonyl chloride (1.0 eq.) with DABCO (2.0 eq.) as the base in DMF at room temperature for 6 h. The reaction mixture was poured into ice-cold dilute aqueous HCl; the sulfonamide usually precipitated from solution and was collected by filtration.

Screening Strategy. Compounds were tested for BRPFs BRD binding (ΔT_m) with a differential scanning fluorimetry (DSF) assay (Table 2). Selected compounds were then screened for inhibition (IC_{50}) of BRPF BRD activity as measured by the BROMO*scan* biochemical assay (Table 3). BRD9 and BRD4(BD1) were routinely used as BRD counter screens to establish evidence of selectivity in both the DSF and BROMO*scan* assays. Preferred compounds were then evaluated for selectivity against a panel of 48 BRDs by DSF and inhibition of BRPF BRD activity was confirmed by independent evaluation by an AlphaScreen biochemical assay (IC_{50}). Finally, equilibrium dissociation constants (K_D) were determined by isothermal titration calorimetry (ITC).

Structure Activity Relationships. The SARs were initially focused on exploring substituents on the phenyl ring of **12** and then modification of the groups at the N1 and C3 positions of the quinolin-2-one core **13**-**15** (Tables 2 and 3). Furthermore, target compounds were designed to have molecular and physicochemical properties consistent with drug-like space. Modulation of the lipophilicity of target compounds was achieved by the application of the lighter halogens (F, Cl), small alkyls (Me, Et), alkoxy (OMe) and nitriles (CN).

In general, there was a good correlation between the DSF and BROMO*scan* data for these compounds with very similar trends in ranked order of affinities. However, as has been noted by others, the BROMO*scan* data routinely showed higher affinities when compared to other quantified endpoints such as the AlphaScreen or ITC measurements.

A more complete analysis of phenyl derivative **12-a** established some modest selectivity over both BRD9 and BRD4(BD1). Introduction of a nitrile at each of the positions of the phenyl ring showed a preference for the 3- and 4- positions, **12-c** and **12-d** respectively, with the 2-CN **12-b** being poorly tolerated. Combining a 4-CN group with a second substituent at either the 2- or 3-positions on the phenyl ring (**12-e,f,g,h**) offered no significant advantage except for the 2-Me,4-CN analogue **12-f**. The 3-Cl,4-Cl compound **12-h** had similar potency to **12-d** but at the expense of increased lipophilicity (ΔcLogP +1.5) and was not pursued .

As had been seen previously with **6** and **7**, once again, a significant improvement in BRPF1 affinity was achieved by the introduction of a 3-Me group on the quinolin-2-one of **12-d** to give **13-d** as the most potent compound so far (BRPF1 IC_{50} 7.9 nM; mw 353; cLogP 2.5; LE = 0.45; LLE = 5.6). Additional screening of **13-d** showed reasonable binding affinity for all three BRPFs with good selectivity over BRD9 (39-fold) and BRD4(BD1) (>500-fold)(Figure S2). The introduction of a 2-MeO group **13-i** also gave a potent inhibitor of BRPF1 activity but, not surprisingly, reintroduced some unwanted BRD4 activity.[29] Compound **13-i** represents our closest structural analogue to **23** and yet **13-i** still shows reasonable selectivity over BRD4(BD1) (60-fold). This selectivity can be attributed to a combination of the intrinsic preference of the quinolin-2-one core **5b** for BRPF1 (Table 1) and the accommodation of the substituent at N1. Limited SARs would suggest that BRD4 prefers a N1-H whereas BRPF1 prefers a N1-Me; this single point change in chemical structure may represent a simple way to switch between BRPF1 and BRD4 activity.

Increasing the size of the 3-alkyl substituent from 3-Me to 3-Et (**14-d**) was poorly tolerated whereas exchanging the N1-Me for an N1-Et (**15-d**) showed similar affinity. Although these simple modifications at C3 and N1 of the quinolin-2-one failed to improve the BRPF1 affinity (*cf* **13-d** v **14-d** v **15-d**), they did provide some evidence of how the affinity could be reduced to identify an inactive close analogue of **13-d** (vide infra).

Preliminary attempts to design a BRPF1 selective inhibitor in the quinolin-2-one template were based upon hybrid structures of **13-d** with **2**. The incorporation of a 6-benzamide and 7-pyrrolidine gave **21** (Table 3) which proved to be a modest inhibitor of BRPF1 (IC_{50} 220 nM; mw 391; cLogP 3.0; LE = 0.32; LLE = 3.7) with only an incremental improvement of selectivity over BRD1 when compared to **13-d** (11- vs 6-fold resp.). However, amide **21** had similar potency for BRD9 (IC_{50} 420 nM) and may be considered as a modest BRPF1-BRD9 dual inhibitor for further optimization.

Around this time, our initial efforts to determine the binding mode of a representative quinolin-2-one sulfonamide to BRPF1B was achieved by the determination of a co-crystal X-structure of BRPF1B with 1,4-dimethylquinolin-2-one **22** (BRPF1 IC_{50} 60 nM; Table 3; Figures 4 and S6).

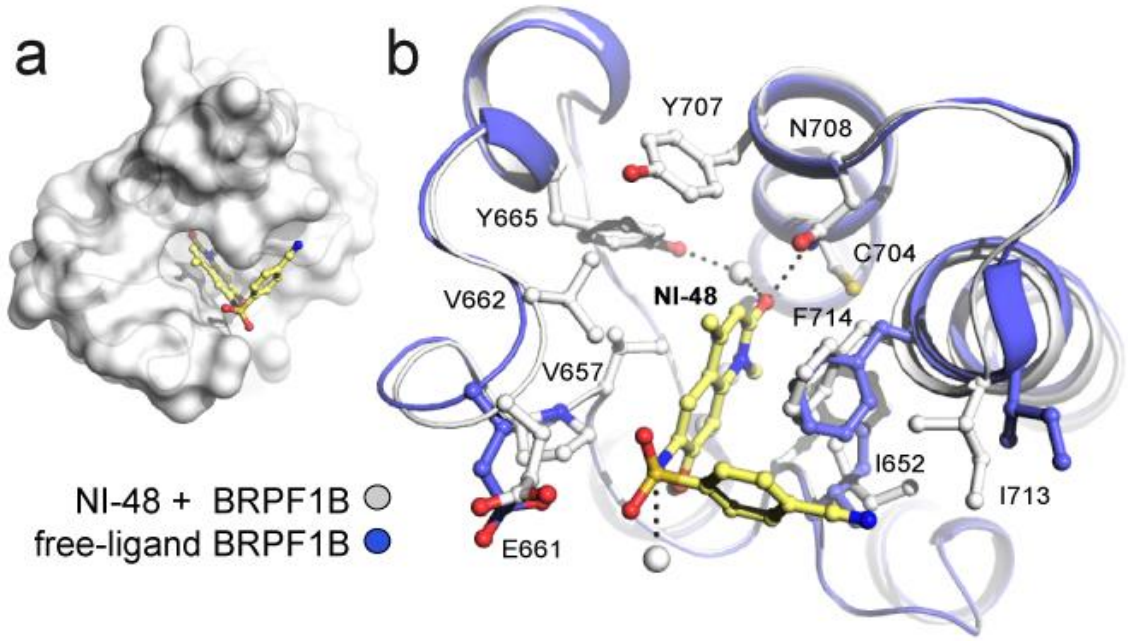

Figure 4. Co-crystal structure of **22** (**NI-48**; reference 38) with BRPF1B bromodomain solved at 1.65 Å (pdb 5T4V). A) Surface representation B) Cartoon representation of the binding site details of **22** (yellow) bound to BRPF1B (grey) and overlaid with ligand-free BRPF1B structure (blue).

Compound **22** occupies part of the substrate acetylated peptide-binding groove of the BRD in good shape complementarity (Figure 4A). The quinolin-2-one scaffold maintains the same conformation as shown for the complex structure with fragment **5b**. However, new features of the binding mode arose with this novel structure. Interestingly, upon binding, the ligand induces a conformational twist of the Phe714 gatekeeper residue. The phenyl side chain forms a parallel, face-centered π-π stacking interaction with the quinolinone core ring at approximately 3.6 Å. Moreover, the new rotamer is pointing towards the benzonitrile ring forming a perpendicular T-shaped C-H-π interaction. This is shown with the structural superposition of the free-ligand BRPF1B structure (Figure 4B). We also observe the nitrile group accommodated to a pre-formed hydrophobic cleft with residue Ile713 at the top of the αC helix. Additional points of interest are that the network of five conserved water molecules in the binding pocket is not altered and the NH group from the sulfonamide is stabilized through an intra-hydrogen bond to the 7-OMe group on the quinolin-2-one (Figure S6).

Table 2: Evaluation of *N*-methylquinolin-2(1*H*)-ones **12**-**15** in DSF ΔT_m shift assay

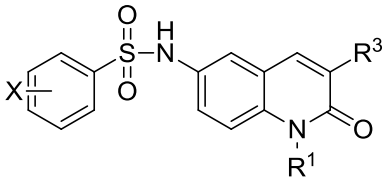

12-15

Compound	R^1	R^3	X	ΔT_m shift at 10 μM (°C)				
				BRPF1	BRPF2 (BRD1)	BRPF3	BRD9	BRD4(BD1)
12-a	Me	H	H	5.3	1.9	1.5	3.5	1.1
12-b	Me	H	2-CN	2.4	0.9		2.9	1.3
12-c	Me	H	3-CN	4.4	2.1		2.5	1.1
12-d	Me	H	4-CN	5.2	2.4		2.3	1.4
12-e	Me	H	2-F; 4-CN	3.6	1.3	1.2		
12-f	Me	H	2-Me; 4-CN	6.5	3.4	2.4	2.2	0.4
12-g	Me	H	3-Cl; 4-CN	4.3				
12-h	Me	H	3-Cl; 4-Cl	4.9	2.5			
13-d	Me	Me	4-CN	9.7	5.1	4.5	3.5	0.95
14-d	Me	Et	4-CN	5.6	3.3			
15-d	Et	Me	4-CN	5.2	1.5	1.2		

Table 3: Evaluation of *N*-methylquinolin-2(1*H*)-ones **12**-**15**, **21** and **22** in the BROMO*scan* assay [a]

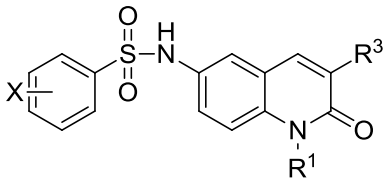

12-15

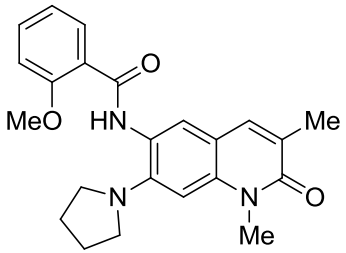

21

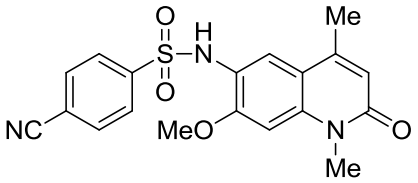

22

Compound	R^1	R^3	X	IC_{50} (nM)				
				BRPF1	BRPF2 (BRD1)	BRPF3	BRD9	BRD4(BD1)
12-a	Me	H	H	65	1400	7600	2200	1700
12-b	Me	H	2-CN	430	1700			
12-c	Me	H	3-CN	56	270			
12-d	Me	H	4-CN	43	200	1000	910	2800
12-g	Me	H	3-Cl; 4-CN	62	450	2300	2500	7200
12-h	Me	H	3-Cl; 4-Cl	44	230			
13-d	Me	Me	4-CN	7.9[b]	48	260	310	4500
13-i	Me	Me	2-OMe	9	130			600
14-d	Me	Et	4-CN	180				
15-d	Et	Me	4-CN	15				
21				220	2600	12000	420	4600
22				60[b]	1800	9300	890	17000

[a] BRD IC_{50} values are geometric means of two experiments (n =2). Differences of <2-fold should not be considered significant. [b] n = 4.

Selectivity of 13-d. Completing the evaluation of lead compound **13-d** against all members of the class IV family of BRDs in the BROMO*scan* assay identified affinity for BRD7 but was completely selective over the ATAD2s (Table 4). **13-d** was confirmed as a potent inhibitor of BRPF1 by independent evaluation in an AlphaScreen biochemical assay and with a very similar relative rank order of activities to other screening formats (Table 4).

Compound **13-d** was then evaluated in a number of assays to establish the broader pharmacological selectivity. **13-d** was screened for BRD binding by DSF against a panel of 48 BRDs and showed excellent selectivity. All activity was confined to the class IV family of BRDs with ΔT_m < 1 ^oC stabilization for all non-class IV BRDs (Figure 5; Table S1). ITC data showed that **13-d** bound the BRD of BRPF1 with an equilibrium dissociation constant, $K_{D,}$ of 40 nM and an enthalpy change, ΔH, of -11.7 kcal mol^{-1} (Table 4; Figure 6). Additional ITC studies showed **13-d** bound the BRD of BRD1 with a K_D of 210 nM, whereas binding to BRPF3 and BRD9 was weaker (Table 4; Figure S3).

Compound **13-d** has reasonable aqueous solubility and good cell permeability as measured by transit performance in the Caco2 cell line but with some evidence of efflux (Table 4). Any cardiovascular risk through direct interaction with cardiac ion channels was low as **13-d** showed minimal activity against a panel of 8 cardiac ion channels in the Eurofins CardiacProfile with only 45.6% normalized inhibition of the hERG current amplitudes at 30 μM (Table S2).

Hence, **13-d** is a biased, potent inhibitor of the BRD of the BRPFs with excellent selectivity over non-class IV BRD proteins.

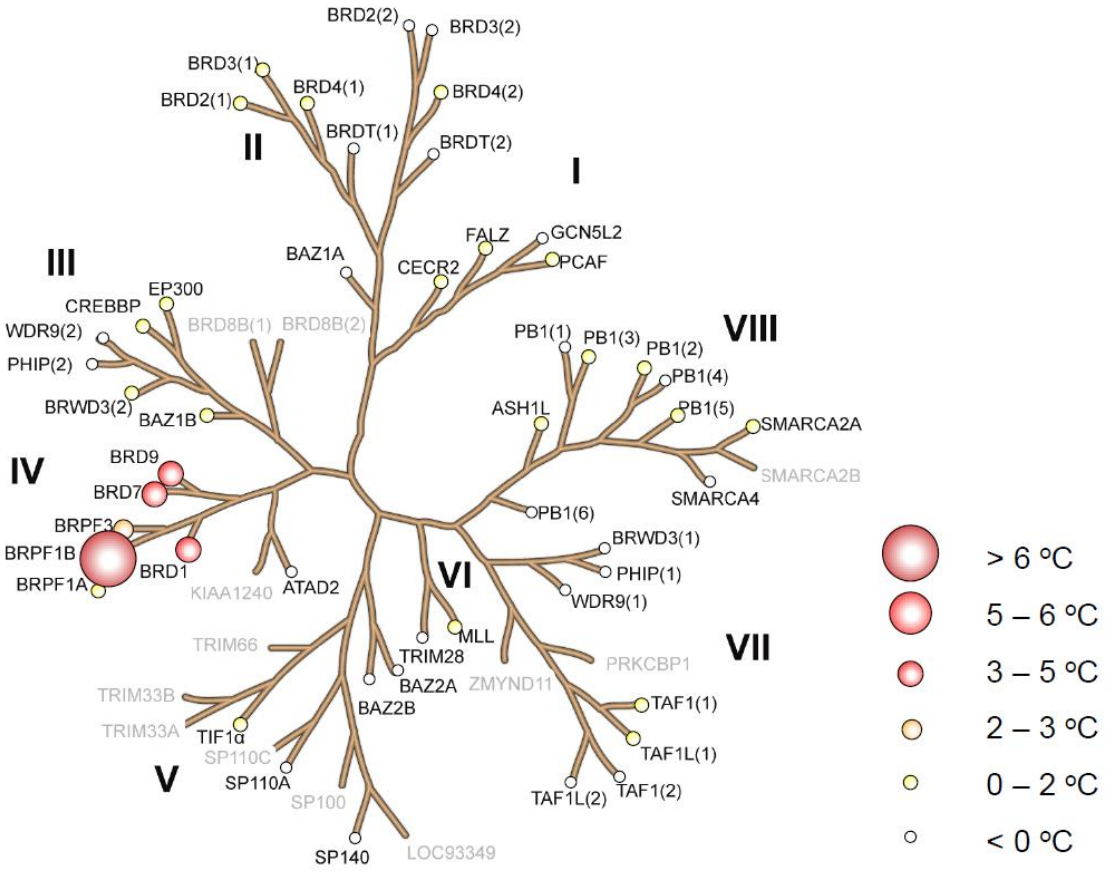

Figure 5. Selectivity profile of **13-d** assessed against 48 BRDs (bold type) by thermal shift, ΔT_m (^oC), at 10 μM as measured by DSF.

Table 4: Summary of physicochemical properties, *in vitro* bromodomain inhibition, ITC screening and cell transit permeability of **13-d**.

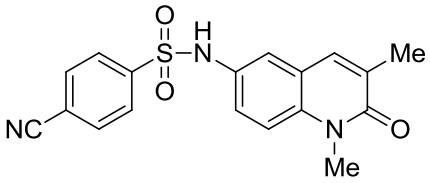

13-d: NI-42

Physicochemical properties			
mw			353
clogP			2.5
tPSA (Å^2)			90
Bromodomain inhibition			
BRPF1/2/3	BROMO*scan*	IC_{50} (nM)	7.9; 48; 260
BRD7/9	BROMO*scan*	IC_{50} (nM)	82; 310
ATAD2A/2B	BROMO*scan*	IC_{50} (nM)	>100,000; >100,000
BRD4(1)	BROMO*scan*	IC_{50} (nM)	4500
BRPF1/2/3	AlphaScreen	IC_{50} (nM)	140; 760; 2000
BRD9	AlphaScreen	IC_{50} (nM)	1100
BRD4(1)	AlphaScreen	IC_{50} (nM)	>20,000
Bromodomain ITC screening			
BRPF1/2/3	ITC	K_D (nM)	40; 210; 940
BRD9	ITC	K_D (nM)	1130
Solubility and cell permeability			
Aqueous solubility			moderate (100 μM min)[a]
Caco2 transit AB/BA, P_{app} (x10^{-6} cms^{-1})			10/50

[a] Maximum concentration used in screening assays created by serial dilution of a 100 mM stock solution of **13-d** in DMSO.

Figure 6: ITC data for **13-d** with BRPF1.

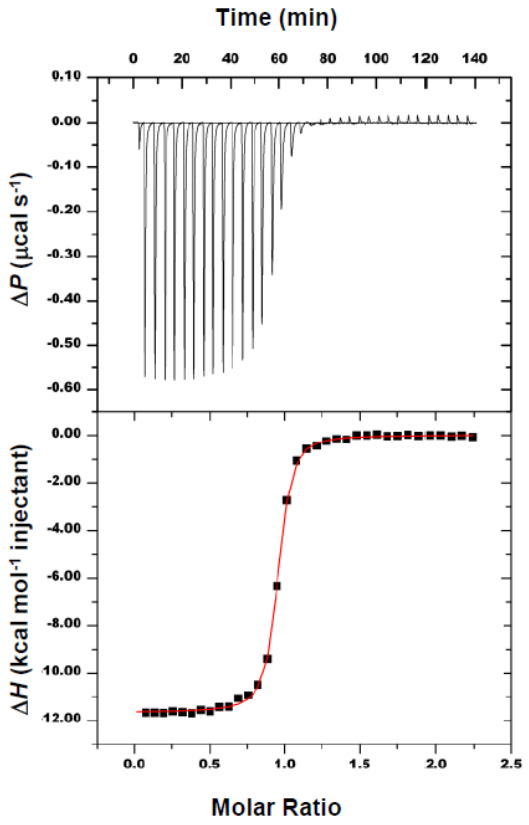

The figure shows raw binding heats for each injection (upper panel) as well as normalized binding enthalpies and a non-linear least squares fit to a single binding site model. The fit revealed K_D = 40 nM, ΔH = -11.7 kcal mol^{-1} and $T\Delta S$ = -1.87 kcal mol^{-1}.

BRPF1B target engagement. Target engagement in living cells was demonstrated in a fluorescence recovery after photobleaching (FRAP) assay[39] using a fusion protein of green fluorescent protein with a triplicated BRD of BRPF1B linked to a nuclear localization signal ectopically expressed in the human osteosarcoma cell line U2OS. The histone deacetylase (HDAC) inhibitor SAHA was used to increase overall levels of histone acetylation resulting in a sufficient window measuring differences in recovery time and demonstrating the acetylation dependence of the FRAP experiments. Compound **13-d** displaced BRPF1B-BRDx3 from chromatin at 1 μM as shown by the significantly reduced recovery time of the BRPF1B-GFP fusion protein (Figure S7). Hence, these FRAP experiments confirm **13-d** inhibits BRPF1B BRDs in the nucleus.

AML cell based activity. Compound **13-d** has been evaluated in a number of cellular models in order to explore a credible link between the BRPF proteins and disease. These cellular models include osteoclastogenesis, inflammation and fibrosis; results from these studies will be reported separately. Our own interest was to explore the potential role of BRPF1 in acute myeloid leukemia (AML) and other cancers.

Table 5. Examples of inhibition of proliferation of AML and other cancer cell lines (GI_{50}) by **13-d**.

Cancer cell line [a]	GI_{50} (μM)
AML cell lines:	
OCI-AML2	1.3
Nomo-1	4.6
THP-1	5.7
KG-1	7.0
MV-4-11	9.9
Non-AML cell lines:	
SW48, NUGC-4, HepG2, COLO 205, OCUM-1, HUP-T4, LOVO, C-99, 22Rv1, SK-CO-1, MOLP-8, OGP-1, AGS, Hs 766t, SNU-5, SW948, RKO, OCI-LY-19, KG-1, Panc02.03, SW403, HCC1187, NCI-H1437, IM-9, AsPC-1, SW620, LS180	1 - 10
~100 cell lines	> 30

[a] AstaZeneca CLIMB panel includes 211 cancer cell lines. 72 h proliferation assay; 9 point dose-response-curve with a highest concentration of 10 or 30 μM (n = 2). For an example of the use of oncology cell panels in mechanistic and pathways analysis, see reference 40.

We treated an indexed cell panel of 211 cancer cell lines (CLIMB panel)[40] with **13-d** for 72 h and observed modest and selective inhibition of proliferation of certain AML cell lines (Table 5). Three of these lines (NOMO-1, THP-1 and MV-4-11) exhibit translocations targeting *MLL*. All five lines either

originate from patients who presented with AML with significant monocytic lineage differentiation at diagnosis (OCI-AML2, NOMO-1, THP-1 and MV-4-11) or have strong latent monocyte/macrophage lineage differentiation potential (KG-1), in response, for example, to phorbol ester.[41] Given the original observation of BPRF1-associated MOZ fusions in myelomonocytic leukaemia,[42] therapeutic targeting of BRPF1 may, in particular, be valuable in the myelomonocytic morphologic subtype of human AML.

Taken together, these results provide clear evidence that **13-d** is active in cellular assays although additional studies will be required to more fully establish the role of **13-d** and the BRPFs in AML.

Pharmacokinetics. Pharmacokinetic data for **13-d** was generated *in vivo* in mouse (Tables 6 and S3A). Following single intravenous administration of **13-d**, clearance was low relative to liver blood flow and volume of distribution was moderate resulting in an elimination half-life of 2.0 h. Single oral administration of **13-d** as a suspension showed good oral bioavailability of 49 % even with incomplete absorption. These results established that **13-d** had pharmacokinetic properties compatible with oral dosing in mouse PK-PD models of disease with a 3 mg/kg p.o. dose achieving *free* drug levels above the BRPF1 K_D (ITC) for 4-5 h (Table S3B).

Table 6: Mouse pharmacokinetic data for **13-d** [a]

Liver microsomes, Cl_{int} (μL/min/mg)	14
Plasma protein binding, f_u	0.03
Intravenous dose (mg/kg)	1.0
Elimination half-life, $T_{1/2}$ (h)	2.0
Blood clearance, Cl (mL/min/kg)	4
Volume of distribution, V_d (L/kg)	0.7
Oral dose (mg/kg)	3.0
C_{max} (μM)	4.0
T_{max} (h)	1.0
$AUC_{0-\infty}$ (ng.h/mL)	5700
Bioavailability, F_{po} (%)	49
Fraction absorbed (%)	51

[a] Female CD-1 mouse (n=3)

Inactive Control. Chemical probes are most valuable when they are partnered with an inactive control to assist with the interpretation of phenotypic assays. Ideally, the inactive control will share a similar chemical structure and physicochemical properties as close as possible to the active compound. Hence we designed a series of close analogues of **13-d** where the key recognition interactions between the quinolone C2-carbonyl with Asn708 and the Tyr665 water network could be disrupted by increasing the size of the alkyl groups flanking the carbonyl and so prevent binding. Incorporation of ethyl groups at *both* N1 and C3 gave **16-d** (cf **14-d** and **15-d**) which removed activity as measured against the BRPFs and a representative set of bromodomains in the BROMO*scan* (>100 μM) and AlphaScreen assays (>20 μM) (Table 7).

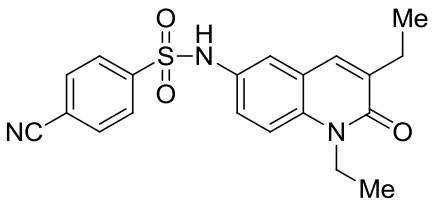

16d
mw 381; clogP 3.5; tPSA 90

Table 7. Inhibition (IC_{50}) of BRD activity for inactive control **16-d**.

	IC_{50} (nM)	BRDs
BROMO*scan* [a]	> 100,000	BRPF1, BRD1, BRPF3, BRD9, BRD7, ATAD2A, ATAD2B, BRD4(BD1), CREBBP, PCAF, BAZ2A, TRIM33, CECR2
	77,000	SMARCA2A
AlphaScreen	> 20,000	BRPF1, BRD9, BRD4(BD1), CECR2, FALZ, TAF1A

[a] BRD IC_{50} values are geometric means of two experiments (n =2).

CONCLUSIONS

We have designed and evaluated a number of new quinolin-2-one derivatives as inhibitors of BRPF BRD activity. Starting with the fragment hit *N*-methylquinolin-2-one (**5b**), which had modest affinity for PCAF, we demonstrated that **5b** had much higher affinity for BRPF1. The preferred binding of **5b** to BRPF1 was rationalized through an X-ray co-crystal structure determination which underpinned future inhibitor design. Optimization of **5b** by incorporation of a 6-phenyl sulfonamide gave **12-a** and preliminary results were encouraging showing reasonable binding affinity for all three BRPFs. SARs established that potent BRPF1 inhibition could be retained through incorporation of various groups on the phenyl ring of the sulfonamide with a 4-CN group preferred (**12-d**). A significant improvement in affinity was achieved by the introduction of a 3-Me group onto the quinolin-2-one of **12-d** to give **13-d** as the most potent compound prepared whilst retaining good physicochemical properties.

Compound **13-d** was then evaluated in a number of assays to establish the broader pharmacological selectivity. **13-d** was screened by DSF against a panel of 48 BRDs and showed excellent selectivity with all activity confined to the class IV family of BRDs. ITC data showed that **13-d** preferentially bound the BRD of BRPF1 and BRD1 whereas binding to BRPF3 and BRD9 was weaker. Based on these results, **13-d** was identified as a biased, potent inhibitor of the BRD of the BRPFs with excellent selectivity over non-class IV BRD proteins. BRPF1 target engagement in living cells was demonstrated in a FRAP assay. Compound **13-d** displaced BRPF1B-BRDx3 from chromatin at 1 μM as shown by the significantly reduced recovery time of the BRPF1B-GFP fusion protein.

Evaluation of **13-d** in a panel of cancer cell lines, including AML lines, showed a modest (GI_{50} 1-10 μM) and selective inhibition of proliferation of certain lines, particularly those lines exhibiting monocytic lineage differentiation. These results provide clear evidence that **13-d** is active in cellular assays. However, additional studies will be required to fully establish the role of **13-d** and the BRPFs in AML.

Pharmacokinetic data for **13-d** was generated *in vivo* in mouse with single oral administration of **13-d** as a suspension showing good oral bioavailability. These results established that **13-d** had pharmacokinetic properties compatible with oral dosing in mouse PK-PD models of disease with a 3 mg/kg p.o. dose achieving *free* drug levels above the BRPF1 K_D for 4-5 h.

In conclusion, we propose that **13-d** is a new, structurally orthogonal chemical probe for the BRPFs suitable for cellular and *in vivo* studies to explore the fundamental biology of these proteins. Chemical probe **13-d** (**NI-42**)[38] will be of most value in the interpretation of phenotypic assays when used in conjunction with the inactive control **16-d** and with other available chemical probes of the class IV BRDs.

EXPERIMENTAL SECTION

Chemistry methods and compound characterization data for 13-d and 16-d.

General Methods:

All anhydrous solvents and reagents were obtained from commercial suppliers and used without further purification. Flash chromatography refers to medium pressure silica gel (C60 (40-60 μm)) column chromatography, unless otherwise stated. The progress of reactions was monitored by thin layer chromatography (TLC) performed on Keiselgel 60 F_{254} (Merck) silica plates and visualised by exposure to UV light at 254 nm.

Melting points (mp) were determined in open capillary tubes on a Stuart SMP10 apparatus and are uncorrected. Infrared (IR) analysis was performed on a Perkin Elmer Spectrum 1000 FT-IR in the 4000-400 cm^{-1} range. ^{1}H Nuclear Magnetic Resonance (^{1}H NMR) spectra were recorded on a Bruker Advance 400 Spectrophotometer at 400 MHz or Bruker Advance 500 Spectrophotometer at 500 MHz. Chemical shifts were measured in parts per million (ppm) relative to tetramethylsilane (δ = 0) using the following internal references: $CDCl_3$ (δ 7.26), CD_3OD (δ 3.32), DMSO-d_6 (δ 2.50). Multiplicities in ^{1}H NMR spectra are quoted as: s = singlet, d = doublet, t = triplet, q = quartet, m = multiplet, dd = double doublet, ddd = double double doublet. ^{13}C Nuclear Magnetic Resonance (^{13}C NMR) spectra were recorded on a Bruker Advance 500 Spectrophotometer at 125 MHz. Chemical shifts were measured in parts per million (ppm) relative to tetramethylsilane (δ = 0) using the following internal references: $CDCl_3$ (δ 77.16), CD_3OD (δ 49.00), DMSO-d_6 (δ 39.52). 2D NMR techniques HSQC, HMQC and HMBC were also utilised for the assignment of ^{1}H and ^{13}C NMR signals. High-resolution mass spectra (HRMS) were recorded on a Thermo Navigator mass spectrometer coupled to an HPLC instrument using electrospray ionisation (ESI) and time-of-flight (TOF) mass spectrometry. Alternatively, HRMS were recorded at the EPSRC UK National Mass Spectrometry Facility (NMSF) at Swansea University. Analytical reverse-phase high-performance liquid chromatography (HPLC) was carried out on a XSELECT™ CSH™ C-18 column (2.5 μm; 6 x 50 mm). HPLC experiments (system A) were performed with gradient conditions: initial fixed composition 5% B to 50% B over 20 min, then increased to 95% B over 2 min, held for 2 min at 95% B, then returned to 5% B in 1 min. Total duration of gradient run was 25 min. Eluents used were solvent A (H_2O with 0.02% TFA) and solvent B (MeCN with 0.02% TFA). Flow rate: 1.00 mL/min.

Purity of screening compounds **12**-**15**, **21** and **22** was evaluated by NMR spectroscopy and HPLC analysis. All compounds had purity ≥ 95 % except **21** which had a purity of 91 % by HPLC.

6-Amino-1,3-dimethyl-6-quinolin-2-(1*H*)-one (**7**). A 500 mL round bottom flask was charged with 1,3-dimethyl-6-nitroquinolin-2-(1*H*)-one (**20**) (5.00 g, 22.9 mmol, 1.0 eq.) and palladium on carbon (5 % wt., 2.44 g, 1.45 mmol, 0.05 eq.). The flask was sealed then evacuated and back-filled with nitrogen three times before adding ethanol (300 mL). The stirred slurry was then re-evacuated until the solvent began to bubble and back-filled with nitrogen once more. A balloon of hydrogen was attached to the flask *via* a syringe fitted with a stop-cock. The flask was evacuated until the solvent began to boil and then back-filled with hydrogen gas five times. The reaction was then stirred for seven hours after which point the complete consumption of starting material was confirmed by TLC. At the end of the reaction, the reaction flask was evacuated and back-filled with nitrogen three times, filtered through a pad of Celite® onto a glass-sintered funnel. The Celite® pad was further washed with ethanol (300 mL) and then the filtrate concentrated under reduced pressure to give 6-amino-1,3-dimethyl-6-quinolin-2-(1*H*)-one (**7**) (4.10 g, 95 %) as a pale yellow solid that was not purified further. ^{1}H NMR (500 MHz, DMSO-d_6): δ 7.55 (s, 1H), 7.21 (d, *J* = 8.8 Hz, 1H), 6.87 (d, *J* = 8.8 Hz, 1H), 6.71 (s, 1H), 5.04 (br. s, 2H), 3.56 (s, 3H) 2.08 (s, 3H); ^{13}C NMR (125 MHz, DMSO-d_6): δ 160.9, 143.6, 135.0, 130.5, 128.7, 120.9, 117.7, 115.0, 110.0, 29.2, 17.5.

4-Cyano-*N*-(1,3-dimethyl-2-oxo-1,2-dihydroquinolin-6-yl)benzenesulfonamide (**13-d**). To a solution of 6-amino-1,3-dimethylquinolin-2(1*H*)-one (**7**) (188 mg, 1.00 mmol) and pyridine (158 mg, 2.00 mmol, 2.0 eq.) in DMF (5 mL) was added 4-cyanobenzenesulfonyl chloride (201 mg, 1.00 mmol, 1.0 eq.) at room temperature and the reaction mixture stirred overnight. The resulting suspension was homogenised by addition of DMF (3 mL), concentrated onto Celite® and purified by column chromatography (acetone:hexane, gradient elution 30:70 to 60:40) to give **13-d** (129 mg, 0.37 mmol, 37%) as a white solid. m.pt. 279-282 ^{o}C (acetone-hexane)**;** ^{1}H NMR (400 MHz, DMSO-d_6): δ 10.52 (1H, s), 8.06 - 8.00 (2H, m), 7.90 - 7.84 (2H, m), 7.73 (1H, s), 7.41 (1H, d, *J* = 9.1 Hz), 7.33 (1H, d, *J* = 2.5 Hz), 7.23 (1H, dd, *J* = 9.1, 2.5 Hz), 3.57 (3H, s), 2.09 (3H, d, *J* = 1.0 Hz); ^{13}C NMR (126 MHz, DMSO-d_6): δ 161.4, 143.3, 136.3, 135.0, 133.5, 130.8, 130.0, 127.4, 123.5, 120.3, 119.9, 117.5, 115.5, 115.3, 29.4, 17.3; HRMS *m/z* (ESI$^+$) found $(M+H)^+$ 354.0908, $C_{18}H_{15}N_3O_3S$ requires $(M+H)^+$ 354.0907; HPLC: Retention time (system A): t_R= 8.97 min. Purity: >95%.

4-Cyano-*N*-(1,3-diethyl-2-oxo-1,2-dihydroquinolin-6-yl)benzenesulfonamide (**16-d**) was prepared according to general procedure as described for **13-d** from 6-amino-1,3-diethylquinolin-2(1*H*)-one (40 mg, 0.18 mmol) with 4-cyanobenzenesulfonyl chloride to give **16-d** (37 mg, 0.09 mmol) as a pale yellow solid. ^{1}H NMR (500 MHz, DMSO-d_6): δ 10.56 (1H, s), 8.04 (2H, d, *J* = 8.5 Hz), 7.89 (2H, d, *J* = 8.5 Hz), 7.68 (1H, s), 7.46 (1H, d, *J* = 8.8 Hz), 7.41 (1H, d, *J* = 2.5 Hz), 7.23 (1H, dd, *J* = 9.1, 2.5 Hz), 4.22 (2H, q, *J* = 6.9 Hz), 1.21 - 1.10 (6H, m), [1xCH_2 overlaps with DMSO]; ^{13}C NMR (126 MHz, DMSO-d_6): δ 160.5, 143.4, 135.3, 134.9, 133.6, 133.5, 130.7, 127.4, 123.6, 120.7, 120.3, 117.5, 115.3, 115.2, 36.9, 23.5, 12.7, 12.5; HRMS *m/z* (ESI$^-$) found $(M-H)^-$ 380.1057, $C_{20}H_{19}N_3O_3S$ requires $(M-H)^-$ 380.1069; HPLC: Retention time (system A): t_R= 10.36 min. Purity: >95%.

3-Methylquinolin-2-(1*H*)-one (**18**). To a stirred solution of 3-methylquinoline (**17**) (25.0 g, 175 mmol, 1.0 eq.) in dichloromethane (875 mL) in a 2 litre round bottom flask at 0 °C was added 3-chloroperbenzoic acid (70 %, 47.3 g, 192 mmol, 1.1 eq.) portionwise over 10 minutes. The resulting solution was allowed to warm to room temperature and then stirred overnight. After completion of the reaction, the solution was washed with sodium hydroxide (1.0 M, 300 mL) and the aqueous phase extracted with dichloromethane (2 x 300 mL). The organic layers were combined, dried over *anhydrous* $MgSO_4$, filtered and the solvent removed under reduced pressure to yield crude 3-methylquinolone-*N*-oxide as a white solid, which was used without further purification.

To a 2 L three-necked round bottom flask fitted with an overhead mechanical stirrer was charged crude 3-methylquinolone-*N*-oxide followed by dichloromethane (430 mL) and aqueous sodium hydroxide solution (1.0 M, 400 mL). The resulting biphasic mixture was cooled to 0 °C and to this was added, under rapid agitation, benzoyl chloride (24.4 mL, 210 mmol, 1.2 eq.) dropwise *via* a side-arm pressure equalised dropping funnel. The suspension was stirred overnight and the resulting heterogeneous solution was diluted with diethyl ether and stirred rapidly for 15 minutes. The resultant precipitate was collected by filtration, washed with diethyl ether (200 mL) and then water (200 mL) and dried under vacuum to give 3-methylquinolin-2(1*H*)-one (**18**) (16.3 g 59 % over 2 steps). ^{1}H NMR (400 MHz, DMSO-d_6): δ 11.72 (br. s, 1H), 7.75 (s, 1H), 7.56 (d, *J* = 7.8 Hz, 1H), 7.41 (t, *J* = 8.3 Hz, 1H), 7.29 (d, *J* = 8.3 Hz, 1H), 7.14 (t, *J* = 7.5 Hz, 1H), 2.09 (s, 3H); ^{13}C NMR (125 MHz, DMSO-d_6): δ 162.4, 137.9, 136.3, 129.8, 129.0, 126.9, 121.6, 119.4, 114.7, 16.5.

1,3-Dimethylquinolin-2-(1*H*)-one (19). To a solution of 3-methylquinolin-2(1*H*)-one (**18**) (16.3 g, 103 mmol, 1.0 eq.) in *anhydrous* DMF (500 mL) in a 1 litre round bottom flask cooled to 0 °C and under an argon atmosphere was added NaH (60 % wt., 4.50 g, 113 mmol, 1.1 eq.) and the reaction mixture stirred for 0.5 hours. Iodomethane (8.3 mL, 133 mmol, 1.3 eq.) was added dropwise *via* syringe and the reaction mixture stirred for 5 hours. Excess sodium hydride was quenched by the addition of water (30 mL) and the solvents removed under reduced pressure. The resultant slurry was taken up in the minimum volume of ethyl acetate and poured onto crushed ice (approximately 200 g). The resultant heterogeneous mixture was stirred rapidly for 15 minutes and then the precipitate collected by filtration, washed with cold diethyl ether (100 mL) and dried under vacuum to give 1,3-dimethylquinolin-2-(1*H*)-one (**19**) (16.9 g, 95 %) as a white powder. ^{1}H NMR (400 MHz, DMSO-d_6): δ 7.78 (s, 1H), 7.63 (dd, J = 7.8, 1.3 Hz, 1H), 7.58–7.53 (m, 1H), 7.50–7.48 (m, 1H), 7.26–7.22 (m, 1H), 3.64 (s, 3H) 2.13 (s, 3H); ^{13}C NMR (125 MHz, DMSO-d_6): δ 161.7, 138.7, 135.5, 129.5, 128.9, 127.7, 121.8, 120.0, 114.3, 29.3, 16.5.

1,3-Dimethyl-6-nitroquinolin-2-(1*H*)-one (**20**). A 500 mL round bottom flask was charged with 1,3-dimethylquinolin-2-(1*H*)-one (**19**) (16.9 g, 97.5 mmol, 1.0 eq.) and cooled to 0 °C. Concentrated sulfuric acid (120 mL) was added and the reaction mixture stirred for 0.5 hours during which time most of the solid dissolved. To the resultant pale red solution, potassium nitrate (10.4 g, 102.4 mmol, 1.05 eq.) was added in two portions. The reaction mixture rapidly turned yellow and was stirred for a further 4 hours, after which it was poured onto crushed ice (approximately 400 g) and stirred rapidly for 0.5 hours. The yellow precipitate was collected by filtration onto a sintered-glass funnel and washed with water (2 x 250 mL). Still on the sintered disk, the resultant filter cake was slurried with hot ethanol (200 mL) using a glass rod and allowed to stand for 10 minutes. The solid was collected by filtration to give 1,3-dimethyl-6-nitroquinolin-2-(1*H*)-one (**20**) (18.5 g, 87 %) as a pale yellow solid. ^{1}H NMR (400 MHz, DMSO-d_6): δ 8.63 (s, 1H), 8.35 (d, J = 8.8 Hz, 1H), 8.03 (s, 1H), 7.7 (d, J = 8.8 Hz, 1H), 3.71 (s, 3H) 2.16 (s, 3H); ^{13}C NMR (125 MHz, DMSO-d_6): δ 161.8, 142.9, 141.4, 135.3, 131.2, 123.9, 123.5, 119.7, 115.7, 30.1, 17.4.

ASSOCIATED CONTENT

Supporting Information

Materials and methods: synthetic procedures and characterisation data for compounds **6** - **22**; DSF, BROMO*scan*™, AlphaScreen™ and ITC determinations; protein crystallization, data collection and structure solution; FRAP assay. Figures: spectroscopic and analytical data for **13-d** and **16-d**; dose-response-curves for **13-d** in BROMO*scan* assay; ITC analysis; BRD protein structures superposition with **5b** and sequence alignment; superposition of BRPF1B histone complex structures and co-structure of BRPF1B with **5b**; experimental electron density map contoured around **22** and ligand interactions map between **22** and BRPF1B; FRAP assay data. Tables: DSF thermal shift selectivity values for **13-d**; IonChannelProfiler™ data; mouse PK determinations; crystal structure data collection and refinement statistics. This material is available free of charge via the Internet at http://pubs.acs.org.

Accession Codes

Coordinates for the X-ray structures of the bromodomain of BRPF1B co-crystalised with fragment *N*-methylquinoline-2(1*H*)-one (**5b**) (5T4U) and **NI-48** (**22**) (5T4V) have been deposited in the Protein Data Bank.

NI-42 (**13-d**) is available from Tocris (cat no. 5786).

AUTHOR INFORMATION

Corresponding author

* PVF: corresponding author at current address: Alzheimer's Research UK UCL Drug Discovery Institute, The Cruciform Building, University College London, Gower Street, London WC1E 6BT, UK. Telephone +44 (0)20 7679 6971. e.mail p.fish@ucl.ac.uk

Notes

The authors declare no competing financial interest.

ACKNOWLEDGMENTS

N.I. is supported by a UCL School of Pharmacy PhD studentship. P.V.F. wishes to thank the UCL School of Pharmacy, UCL Faculty of Life Sciences, and UCL Business for financial support. We thank Jeremy Hunt, Aimee Allen, Dan Treiber and the screening team at DiscoverX Corp. for measuring inhibitor IC_{50} values in the BROMO*scan*™ assay, and the AstraZeneca Oncology screening group for evaluation of NI-42 in a panel of cancer cell lines (CLIMB panel). HRMS were recorded at the EPSRC UK National Mass Spectrometry Facility (NMSF) at Swansea University.

The SGC is a registered charity (number 1097737) that receives funds from AbbVie, Bayer Pharma AG, Boehringer Ingelheim, Canada Foundation for Innovation, Eshelman Institute for Innovation, Genome Canada through Ontario Genomics Institute, Innovative Medicines Initiative (EU/EFPIA) [ULTRA-DD grant no. 115766], Janssen, Merck & Co., Novartis Pharma AG, Ontario Ministry of Economic Development and Innovation, Pfizer, São Paulo Research Foundation-FAPESP, Takeda, and the Wellcome Trust.

ABBREVIATIONS USED

AML, acute myeloid leukemia; ATAD2, ATPase family, AAA domain containing; BRD4(BD1), bromodomain containing protein 4, first bromodomain; BET, bromodomain and extra terminal domain; BRD, bromodomain containing protein; BRPF, bromodomain and PHD finger-containing; CLIMB, Cell Lines Indexed for Molecular Biology; DABCO, 1,4-diazabicyclo[2.2.2]octane; DSF, differential scanning fluorimetry; DMF, *N,N*-dimethyl formamide; EAF6, EAS1-associated factor 6; EPC, enhancer of polycomb; FRAP, fluorescence recovery after photobleaching; HAT, histone acyl transferase; HBO1, histone acetyltransferase binding to ORC 1 (KAT7); HOX, homeotic; ING5, inhibitor of growth family, member 5; ITC, isothermal titration calorimetry; LE, ligand efficiency = 1.4(-log IC_{50})/number of heavy atoms; LLE, lipophilic ligand efficiency = (-log IC_{50}) - clogP; *m*CPBA, 3-chloroperbenzoic acid; MLL, mixed-lineage leukemia; MORF, monocytic leukemia zinc finger protein-related factor (KAT6B); MOZ, monocytic leukemia zinc finger (KAT6A); NPM1, Nucleophosmin 1;

PCAF, P300/CBP-associated factor; PK-PD, pharmacokinetic-pharmacodynamic; PWWP, Pro-Trp-Trp-Pro; RUNX1, Runt-related transcription factor 1; SAR, structure activity relationship; TIF2, transcriptional mediators/intermediary factor 2; TRIM24, tripartite motif containing 24; WPF, Trp-Pro-Phe.

REFERENCES

1. Brown, P.J.; Müller, S. Open access chemical probes for epigenetic targets. *Future Med. Chem.* **2015**, *7*, 1901-1917.

2. Vidler, L.R.; Filippakopoulos, P.; Fedorov, O.; Picaud, S.; Martin, S.; Tomsett, M.; Woodward, H.; Brown, N.; Knapp, S.; Hoelder S. Discovery of novel small-molecule inhibitors of BRD4 using structure-based virtual screening. *J. Med. Chem.* **2013**, *56*, 8073-8088.

3. Filippakopoulos, P.; Qi, J.; Picaud, S.; Shen, Y.; Smith, W. B.; Fedorov, O.; Morse, E. M.; Keates, T.; Hickman, T. T.; Felletar, I.; Philpott, M.; Munro, S.; McKeown, M. R.; Wang, Y.; Christie, A. L.; West, N.; Cameron, M. J.; Schwartz, B.; Heightman, T. D.; La Thangue, N.; French, C. A.; Wiest, O.; Kung, A. L.; Knapp, S.; Bradner, J. E. Selective inhibition of BET bromodomains. *Nature* **2010**, *468*, 1067-1073.

4. Nicodeme, E.; Jeffrey, K. L.; Schaefer, U.; Beinke, S.; Dewell, S.; Chung, C. W.; Chandwani, R.; Marazzi, I.; Wilson, P.; Coste, H.; White, J.; Kirilovsky, J.; Rice, C. M.; Lora, J. M.; Prinjha, R. K.; Lee, K.; Tarakhovsky, A. Suppression of inflammation by a synthetic histone mimic. *Nature* **2010**, *468*, 1119-1123.

5. Filippakopoulos, P.; Knapp, S. Targeting bromodomains: epigenetic readers of lysine acetylation. *Nat. Rev. Drug Disc.* **2014**, *13*, 337-356.

6. Theodoulou, N.H.; Tomkinson, N.C.; Prinjha, R.K.; Humphreys, P.G. Progress in the development of non-BET bromodomain chemical probes. *ChemMedChem.* **2016**, *11*, 477-487.

7. (a) Romero, F.A.; Taylor, A.M.; Crawford, T.D.; Tsui, V.; Côté, A.; Magnuson, S. Disrupting acetyl-lysine recognition: progress in the development of bromodomain Inhibitors. *J. Med. Chem.* **2016**, *59*, 1271-1298. (b) Zhang, G.; Smith, S. G.; Zhou, M.-M. Discovery of chemical inhibitors of human bromodomains. *Chem. Rev.* **2015**, *115*, 11625-11668. (c) Brand, M.;

Measures, A. M.; Wilson, B. G.; Cortopassi, W. A.; Alexander, R.; Höss, M.; Hewings, D. S.; Rooney, T. P. C.; Paton, R. S.; Conway, S. J. Small molecule inhibitors of bromodomain−acetyl-lysine Interactions. *ACS Chem. Biol.* **2015**, *10*, 22-39. (d) Galdeano, C.; Ciulli, A. Selectivity on-target of bromodomain chemical probes by structure guided medicinal chemistry and chemical biology. *Future Med. Chem*. **2016**, *8*, 1655-1680.

8. Workman**,** P**.;** Collins**,** I. Probing the probes: fitness factors for small molecule tools. *Chem. Biol.* **2010**, *17*, 561-577.

9. Arrowsmith, C. H.; Audia, J. E.; Austin, C.; Baell, J.; Bennett, J.; Blagg, J.; Bountra, C.; Brennan, P. E.; Brown, P. J.; Bunnage, M. E.; Buser-Doepner, C.; Campbell, R. M.; Carter, A. J.; Cohen, P.; Copeland, R. A.; Cravatt, B.; Dahlin, J. L.; Dhanak, D.; Edwards, A. M.; Frederiksen, M.; Frye, S. V.; Gray, N.; Grimshaw, C. E.; Hepworth, D.; Howe, T.; Huber, K. V.; Jin, J.; Knapp, S.; Kotz, J. D.; Kruger, R. G.; Lowe, D.; Mader, M. M.; Marsden, B.; Mueller-Fahrnow, A.; Muller, S.; O'Hagan, R. C.; Overington, J. P.; Owen, D. R.; Rosenberg, S. H.; Roth, B.; Ross, R.; Schapira, M.; Schreiber, S. L.; Shoichet, B.; Sundstrom, M.; Superti-Furga, G.; Taunton, J.; Toledo-Sherman, L.; Walpole, C.; Walters, M. A.; Willson, T. M.; Workman, P.; Young, R. N.; Zuercher, W. J. The promise and peril of chemical probes. *Nat. Chem. Biol.* **2015**, *11*, 536-541.

10. Filippakopoulos, P.; Picaud, S.; Mangos, M.; Keates, T.; Lambert, J. P.; Barsyte-Lovejoy, D.; Felletar, I.; Volkmer, R.; Muller, S.; Pawson, T.; Gingras, A. C.; Arrowsmith, C. H.; Knapp, S. Histone recognition and large-scale structural analysis of the human bromodomain family. *Cell* **2012**, *149*, 214-231.

11. Vezzoli, A.; Bonadies, N.; Allen, M. D.; Freund, S. M.; Santiveri, C. M.; Kvinlaug, B. T.; Huntly, B. J.; Gottgens, B.; Bycroft, M. Molecular basis of histone H3K36me3 recognition by the PWWP domain of Brpf1. *Nat. Struct. Mol. Biol.* **2010**, *17*, 617-619.

12. Poplawski, A.; Hu, K.; Lee, W.; Natesan, S.; Peng, D.; Carlson, S.; Shi, X.; Balaz, S.; Markley, J. L.; Glass, K. C. Molecular insights into the recognition of N-terminal histone modifications by the BRPF1 bromodomain. *J. Mol. Biol.* **2014**, *426*, 1661-1676.

13. Yang, X. J. MOZ and MORF acetyltransferases: Molecular interaction, animal development and human disease. *Biochim. Biophys. Acta* **2015**, *1853*, 1818-1826.

14. Lalonde, M. E.; Avvakumov, N.; Glass, K. C.; Joncas, F. H.; Saksouk, N.; Holliday, M.; Paquet, E.; Yan, K.; Tong, Q.; Klein, B. J.; Tan, S.; Yang, X. J.; Kutateladze, T. G.; Cote, J. Exchange of associated factors directs a switch in HBO1 acetyltransferase histone tail specificity. *Genes Dev.* **2013**, *27*, 2009-2024.

15. Camos, M.; Esteve, J.; Jares, P.; Colomer, D.; Rozman, M.; Villamor, N.; Costa, D.; Carrio, A.; Nomdedeu, J.; Montserrat, E.; Campo, E. Gene expression profiling of acute myeloid leukemia with translocation t(8;16)(p11;p13) and MYST3-CREBBP rearrangement reveals a distinctive signature with a specific pattern of HOX gene expression. *Cancer Res.* **2006**, *66*, 6947-6954.

16. Ullah, M.; Pelletier, N.; Xiao, L.; Zhao, S.P.; Wang, K.; Degerny, C.; Tahmasebi, S.; Cayrou, C.; Doyon, Y.; Goh, S.L.; Champagne, N.; Côté, J.; Yang, X.J. Molecular architecture of quartet MOZ/MORF histone acetyltransferase complexes. *Mol. Cell Biol*. **2008**, *28*, 6828-6843.

17. You, L.; Li L.; Zou, J.; Yan, K.; Belle, J.; Nijnik, A.; Wang, E.; Yang, X.J. BRPF1 is essential for development of fetal hematopoietic stem cells. *J. Clin. Invest.* **2016**, *126*, 3247-3262.

18. Shima, H.; Yamagata, K.; Aikawa, Y.; Shino, M.; Koseki, H.; Shimada, H.; Kitabayashi I. Bromodomain-PHD finger protein 1 is critical for leukemogenesis associated with MOZ-TIF2 fusion. *Int J. Hematol.* **2014**, *99*, 21-31.

19. Barretina, J.; Caponigro, G.; Stransky, N.; Venkatesan, K.; Margolin, A.A.; Kim, S.; Wilson, C.J.; Lehár, J.; Kryukov, G.V.; Sonkin, D.; Reddy, A.; Liu, M.; Murray, L.; Berger, M.F.; Monahan, J.E.; Morais, P.; Meltzer, J.; Korejwa, A.; Jané-Valbuena, J.; Mapa, F.A.; Thibault, J.; Bric-Furlong, E.; Raman, P.; Shipway, A.; Engels, I.H.; Cheng, J.; Yu, G.K.; Yu, J.; Aspesi, P. Jr.; de Silva, M.; Jagtap, K.; Jones, M.D.; Wang, L.; Hatton, C.; Palescandolo, E.; Gupta, S.; Mahan, S.; Sougnez, C.; Onofrio, R.C.; Liefeld, T.; MacConaill, L.; Winckler, W.; Reich, M.; Li, N.; Mesirov,J.P.; Gabriel, S.B.; Getz, G.; Ardlie, K.; Chan, V.; Myer, V.E.; Weber, B.L.; Porter, J.; Warmuth, M.; Finan, P.; Harris, J.L.; Meyerson, M.; Golub, T.R.; Morrissey, M.P.; Sellers, W.R.; Schlege,l R.; Garraway, L.A. The Cancer Cell Line Encyclopedia enables predictive modelling of anticancer drug sensitivity. *Nature* **2012**, *483*, 603-607.

20. Somerville, T.D.; Wiseman, D.H.; Spencer, G.J.; Huang, X.; Lynch, J.T.; Leong, H.S.; Williams, E.L.; Cheesman, E.; Somervaille, T.C. Frequent derepression of the mesenchymal transcription factor gene FOXC1 in acute myeloid leukemia. *Cancer Cell.* **2015**, *28*, 329-342.

21. Kent, W.J.; Sugnet, C.W.; Furey, T.S.; Roskin, K.M.; Pringle, T.H.; Zahler, A.M.; Haussler, D. The human genome browser at UCSC. *Genome Res.* **2002**, *12*, 996-1006.

22. Kitabayashi, I.; Aikawa, Y.; Nguyen, L.A.; Yokoyama, A.; Ohki, M. Activation of AML1-mediated transcription by MOZ and inhibition by the MOZ-CBP fusion protein. *EMBO J*. **2001**, *20*, 7184-7196.

23. OF-1. A chemical probe for the BRPF bromodomains. http://www.thesgc.org/chemical-probes/OF-1 (accessed October 10, 2016).

24. PFI-4. A chemical probe for BRPF1B. http://www.thesgc.org/chemical-probes/PFI-4 (accessed October 10, 2016).

25. Demont, E.H.; Bamborough, P.; Chung, C.W.; Craggs, P.D.; Gordon, L.J.; Grandi, P.; Hobbs, C.I.; Hussain, J.; Jones, E.J.; Le Gall, A.; Michon, A.M.; Mitchell, D.J.; Prinjha, R.K.; Roberts,

A.D.; Sheppard, R.J.; Watson, R.J. 1,3-Dimethyl benzimidazolones are potent, selective inhibitors of the BRPF1 bromodomain. *ACS Med. Chem. Lett.* **2014**, *5*, 1190-1195.

26. Bamborough, P.; Barnett, H.A.; Becher, I.; Bird, M.J.; Chung, C.W.; Craggs, P.D.; Demont, E.H.; Diallo, H.; Fallon, D.J;. Gordon, L.J.; Grandi, P.; Hobbs, C.I.; Hooper-Greenhill, E.; Jones, E.J.; Law, R.P.; Le Gall, A.; Lugo, D.; Michon, A.M.; Mitchell, D.J.; Prinjha, R.K.; Sheppard, R.J.; Watson, A.J.; Watson, R.J. GSK6853, a chemical probe for inhibition of the BRPF1 bromodomain. *ACS Med. Chem. Lett.* **2016**, *7*, 552-557.

27. (a) Palmer, W.S.; Poncet-Montange, G.; Liu, G.; Petrocchi, A.; Reyna, N.; Subramanian, G.; Theroff, J.; Yau, A.; Kost-Alimova, M.; Bardenhagen, J.P.; Leo, E.; Shepard, H.E.; Tieu, T.N.; Shi, X.; Zhan, Y.; Zhao, S.; Barton, M.C.; Draetta, G.; Toniatti, C.; Jones, P.; Geck Do, M.; Andersen, J.N. Structure-guided design of IACS-9571, a selective high-affinity dual TRIM24-BRPF1 bromodomain inhibitor. *J. Med. Chem.* **2016**, *59*, 1440-1454. (b) Bennett, J.; Fedorov, O.; Tallant, C.; Monteiro, O.; Meier, J.; Gamble, V.; Savitsky, P.; Nunez-Alonso, G.A.; Haendler, B.; Rogers, C.; Brennan, P.E.; Müller, S.; Knapp, S. Discovery of a chemical tool inhibitor targeting the bromodomains of TRIM24 and BRPF. *J. Med. Chem.* **2016**, *59*, 1642-1647.

28. Chaikuad, A.; Lang, S.; Brennan, P.E.; Temperini, C.; Fedorov, O.; Hollander, J.; Nachane, R.; Abell, C.; Müller, S.; Siegal, G.; Knapp, S. Structure-based identification of inhibitory fragments targeting the p300/CBP-Associated Factor bromodomain. *J. Med. Chem.* **2016**, *59*, 1648-1653.

29. Wu, J.; Shin, J.; Williams, C.M.M.; Geoghegan, K.F.; Wright, S.W.; Limburg, D.C.; Sahasrabudhe, P.; Bonin, P.D.; Lefker, B.A.; Ramsey, S.J. Design and chemoproteomic functional characterization of a chemical probe targeted to bromodomains of BET family proteins. *Med. Chem. Commun.* **2014**, *5*, 1871-1878.

30. Clark, P.G.; Vieira, L.C.; Tallant, C.; Fedorov, O.; Singleton, D.C.; Rogers, C.M.; Monteiro, O.P.; Bennett, J.M.; Baronio, R.; Müller, S.; Daniels, D.L.; Méndez, J.; Knapp, S.; Brennan,

P.E.; Dixon, D.J. LP99: Discovery and synthesis of the first selective BRD7/9 bromodomain inhibitor. *Angew. Chem. Int. Ed. Engl.* **2015**, *54*, 6217-6221.

31. (a) Chaikuad, A.; Petros, A.M.; Fedorov, O.; Xu, J.; Knapp, S. Structure-based approaches towards identification of fragments for the low-druggability ATAD2 bromodomain. *Med. Chem. Commun. 2014*, *5*, 1843-1848. (b) Demont, E.H.; Chung, C.W.; Furze, R.C.; Grandi, P.; Michon, A.M.; Wellaway, C.; Barrett, N.; Bridges, A.M.; Craggs, P.D.; Diallo, H.; Dixon, D.P.; Douault, C.; Emmons, A.J.; Jones, E.J.; Karamshi, B.V.; Locke, K.; Mitchell, D.J.; Mouzon, B.H.; Prinjha, R.K.; Roberts, A.D.; Sheppard, R.J.; Watson, R.J.; Bamborough, P. Fragment-based discovery of low-micromolar ATAD2 bromodomain inhibitors. *J. Med. Chem.* **2015**, *58*, 5649-5673.

32. Leung, C.S.; Leung, S.S.F.; Tirado-Rives, J.; Jorgensen, W.L. Methyl effects on protein–ligand binding. *J. Med. Chem*. **2012**, *55*, 4489–4500.

33. Lubula, M.Y., Eckenroth, B.E., Carlson, S., Poplawski, A., Chruszcz, M., Glass, K.C. Structural insights into recognition of acetylated histone ligands by the BRPF1 bromodomain. *Febs Lett.* **2014**, *588*, 3844-3854.

34. Fish, P.V.; Filippakopoulos, P.; Bish, G.; Brennan, P.E.; Bunnage, M.E.; Cook, A.S.; Federov, O.; Gerstenberger, B.S.; Jones, H.; Knapp, S.; Marsden, B.; Nocka, K.; Owen, D.R.; Philpott, M.; Picaud, S.; Primiano, M.J.; Ralph, M.J.; Sciammetta, N.; Trzupek, J.D. Identification of a chemical probe for bromo and extra C-terminal bromodomain inhibition through optimization of a fragment-derived hit. *J. Med. Chem.* **2012**, *55*, 9831-9837.

35. www.discoverx.com/bromo-data-sheets (accessed September 15, 2016).

36. Edwards, A.M.; Bountra, C.; Kerr, D.J.; Willson, T.M. Open access chemical and clinical probes to support drug discovery. *Nat. Chem. Biol.* **2009**, *5*, 436-440.

37. Fish, P.V.; Cook, A.S.; Phillips, C.; Bent, A.F.; Mills, J.E.J.; Sciammetta, N. Preparation of novel heterocyclic compounds as bromodomain inhibitors. PCT Int. Appl. WO 2013027168 A1, 2013.

38. Fish, P.V.; Igoe, N.; Bayle, E.D. Preparation of quinolones as inhibitors of class IV bromodomain proteins for cancer therapy. PCT Int. Appl. WO 2016034512 A1, 2016.

39. Philpott, M.; Rogers, C.M.; Yapp, C.; Wells, C.; Lambert, J.P.; Strain-Damerell, C.; Burgess-Brown, N.A.; Gingras, A.C.; Knapp, S.; Müller, S. Assessing cellular efficacy of bromodomain inhibitors using fluorescence recovery after photobleaching. *Epigen. Chromatin* **2014**, 7: 14.

40. Dry, J.R.; Pavey, S.; Pratilas, C.A.; Harbron, C.; Runswick, S.; Hodgson, D.; Chresta, C.; McCormack, R.; Byrne, N.; Cockerill, M.; Graham, A.; Beran, G.; Cassidy, A.; Haggerty, C.; Brown, H.; Ellison, G.; Dering, J.; Taylor, B.S.; Stark, M.; Bonazzi, V.; Ravishankar, S.; Packer, L.; Xing, F.; Solit, D.B.; Finn, R.S.; Rosen, N.; Hayward, N.K.; French, T.; Smith, P.D. Transcriptional pathway signatures predict MEK addiction and response to selumetinib (AZD6244). *Cancer Res.*, **2010**, *70*, 2264-2273.

41. www.dsmz.de/de/kataloge/catalogue (accessed August 23, 2016).

42. Borrow, J.; Stanton, V.P. Jr.; Andresen, J.M.; Becher, R.; Behm, F.G.; Chaganti, R.S.; Civin, C.I.; Disteche, C.; Dubé, I.; Frischauf, A.M.; Horsman, D.; Mitelman, F.; Volinia, S.; Watmore, A.E.; Housman, D.E. The translocation t(8;16)(p11;p13) of acute myeloid leukaemia fuses a putative acetyltransferase to the CREB-binding protein. *Nat. Genet.* **1996**, *14*, 33-41.

Table of Contents Graphic

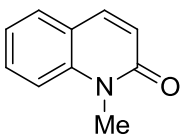

Fragment hit 5b
BRPF1: IC_{50} 4800 nM
LE 0.62; LLE 4.0

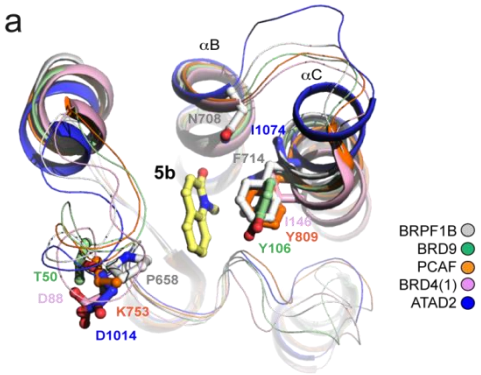

SAR evolution
SBDD

Physicochem. properties

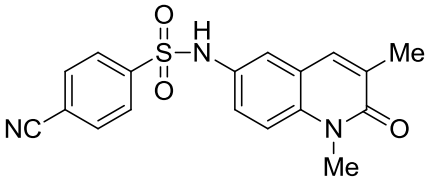

13-d
BRPF1: IC_{50} 7.9 nM
LE 0.45; LLE 5.6
Suitable for cellular and *in vivo* studies